International Journal of Control, Automation and Systems 18(1) (2020) 150-162
http://dx.doi.org/10.1007/s12555-019-0244-9
ISSN:1598-6446 eISSN:2005-4092
http://www.springer.com/12555

Virtual Reality-based Control of Robotic Endoscope in Laparoscopic Surgery

Yeeun Jo, Yoon Jae Kim, Minwoo Cho, Chiwon Lee, Myungjoon Kim, Hye-Min Moon, and Sungwan Kim*

Abstract: Robotic laparoscopic surgery has provided various benefits, but during the surgery, the surgeons are experiencing uncomfortable positioning issue which leads to neck pain and back pain. So, for an enhanced & efficient ergonomic robot-assisted surgery, a novel virtual reality (VR)-based endoscope control system (ECS) is proposed in this research. The overall system in this study is composed of a da Vinci research kit (dVRK), 4-degree-of-freedom ECS, three-dimensional endoscope, and VR headset with a built-in attitude and heading reference system (AHRS) module. Also, the proposed VR headset could replace a stereo viewer in the dVRK which could reduce the size of surgical robot system. Furthermore, the three dimensional endoscope could be controlled by a built-in AHRS module in the VR headset. The proposed system has been verified with four novice volunteers. They showed rapid learning through the peg-transfer task. Additionally, a collision avoidance strategy for VR-based ECS control was developed and verified by performing computer-based simulations. The ergonomic VR-based ECS proposed in this research could greatly reduce surgeon's pains in both neck and back which potentially reduce surgeon's workload during the surgery.

Keywords: Collision avoidance, dVRK, ergonomic system, robot-assisted surgery, virtual reality.

1. INTRODUCTION

Robot-assisted surgical systems that enable minimally invasive surgery (MIS) have made great advances since the first surgical robot was introduced in 1994 [1]. MIS has numerous advantages, such as minimal scarring, little pain, low risk of infection, and short recovery time, and simultaneously overcomes the limitations of MIS performed via the existing robotic techniques [2]. Although efforts are being made to overcome the limitations of conventional MIS systems, such as the long learning period, limited number of degrees of freedom (DOF), and limited complexity of the surgical process [3–6], robot-assisted surgical systems still need further improve to solve issues such as the high purchase and maintenance costs, discontinuous surgical procedures, and the lack of haptic feedback [7–10].

Among these issues, discontinuous surgical procedures occur because two slave systems are controlled by only one master system in the current surgical robot. Due to the control mechanism, the surgeon must separate the temporal stage to control two slave systems, the patient-side manipulator (PSM) and endoscopic systems [11]. This separation can lead to several problems, such as prolonged operation time, collision between surgical tools, and a higher chance of patient injury [12].

Thus, several novel master interfaces to control the endoscopic systems of surgical robots have been proposed. Signal input methods based on hand manipulation (via a joystick, a keyboard, or an innovative novel master interface) [13,14], eye gaze [15], and foot movement [16] have been reported on. Additionally, the concept of a head-mounted interface, consisting of 27 pressure sensors for classifying user intentions and one Hall sensor for activation, was proposed [12]. The pressure sensors were located in the forehead region, and the pattern of pressure values was used to classify the control intention using a support vector machine. However, this method depends on the geometric differences of the human face and requires strong pressure for accurate classification.

Manuscript received April 1, 2019; revised August 4, 2019; accepted August 13, 2019. Recommended by Guest Editors Doo Yong Lee (KAIST) and Jaesoon Choi (Asan Medical Center). This work was supported by the National Research Foundation of Korea grant funded by the Korea government (MSIP) (Grant 2017R1A2B2006163) and by the Korean Electrotechnology Research Institute (KERI) (19-12-N0101-90). The da Vinci Research Kit was donated by Intuitive Surgical, Inc. (Sunnyvale, CA, USA) in 2014.

Yeeun Jo, Minwoo Cho, and Hye-Min Moon are with the Program for Bioengineering, Seoul National University, 103, Daehak-ro, Jongno-gu, Seoul 03080, Korea (e-mails: whdpdms0313@snu.ac.kr, binu6666@naver.com, hmoon00@snu.ac.kr). Yoon Jae Kim (co-first author) is with the Institute of Medical and Biological Engineering, Seoul National University, Seoul 08826, Korea (e-mail: yoonjaekim@snu.ac.kr). Chiwon Lee and Myungjoon Kim are with the Korea Electrotechnology Research Institute, Ansan 15588, Korea (e-mails: chiwonlee@keri.re.kr, mjkim92@keri.re.kr). Sungwan Kim is with the Institute of Medical and Biological Engineering, Seoul National University, and Department of Biomedical Engineering, Seoul National University College of Medicine, Seoul 03080, Korea (e-mail: sungwan@snu.ac.kr).
* Corresponding author

Furthermore, the da Vinci surgical system, a robotic surgical system used the most in robotic MIS, has a ergonomic issue. During the surgery, the surgeons are experiencing uncomfortable positioning issue which leads to neck pain and back pain [17].

Consequently, for an enhanced and efficient ergonomic robot-assisted surgery, a novel virtual reality (VR)-based endoscope control system (ECS) is proposed in this research. Zinchenko et al. also reported on a VR-based control system, considering it to be a highly intuitive and uncontrained system [18]. No pressure sensor is needed in this system because a VR headset contains an attitude and heading reference system (AHRS). The roll, pitch, and yaw angles of the endoscope are controlled when the orientation data of the VR headset becomes larger than the threshold parameters. Furthermore, VR-based robotic surgery eliminates the need for a stereo viewer by streaming the video of the surgical site to the VR headset rather than a stereo viewer. However, the system does not consider velocity control and collision avoidance.

Collision avoidance is particularly important in VR-based control of surgical systems because unintended motion of the head of the user and an incomplete control scheme can lead to serious injury to the patient. In addition, since the camera is attached to the end of the endoscope, it is difficult to judge the situation around the abdomianl cavity. Thus, a collaborative control approach that both reflects the intention of the user and includes a collision avoidance algorithm is required for safe operation.

To address these issues, a VR-based ECS with velocity control strategies and collision avoidance was developed in this study. The intuitiveness of the proposed VR-based ECS was validated with a peg transfer task and line tracking test, and the safety of the system was verified using computer based simulation of collision avoidance algorithm. The VR headset is more ergonomic than the current stereo viewer in da Vinci surgical system so it can greatly reduce surgeon's pains which potentially prevent medical accidents during the surgery. Also, by eliminating a stereo viewer, the volume of the overall surgical robot system could be reduced.

2. METHODS

2.1. Hardware architecture

The hardware configuration of the VR-based ECS for robotic laparoscopic surgery is illustrated in Fig. 1. It consists of a da Vinci® research kit (dVRK, Intuitive Surgical, Inc., Sunnyvale, CA, USA), 4-DOF ECS, three-dimensional (3D) endoscope, and VR headset with a built-in AHRS module. The dVRK is a collection of first-generation da Vinci components and provides a research environment for robotic surgery. It includes two master tool manipulators, two PSMs, a stereo viewer, and

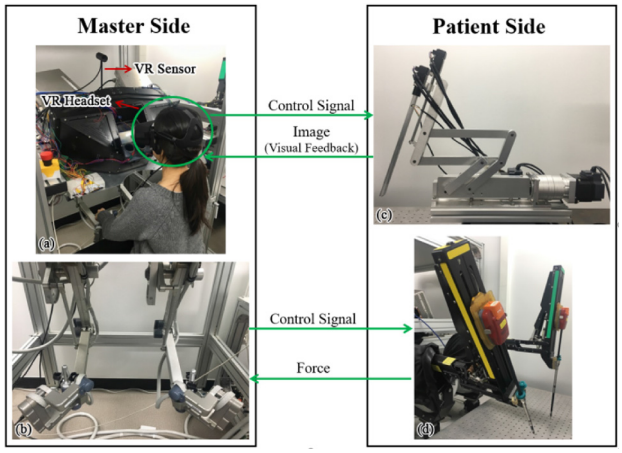

Fig. 1. Hardware configuration of the VR-based ECS.

a foot pedal tray. There is no endoscope system in the dVRK to acquire videos of surgical sites, so the 4-DOF ECS and simple 3D endoscope are employed to provide stereo vision to the user in this system. The 4-DOF ECS shaped into a double parallel link structure was utilized to facilitate 4-DOF rotation based on the point motion of the fulcrum. The 4-DOF ECS is operated with LabVIEW® (LabVIEW® 2015, National Instrument Austin, TX, USA) and its detailed information was described in the previous paper [14].

The simple 3D endoscope for providing visual feedback consists of two complementary metal-oxide-semiconductor (CMOS) camera modules (CMT-1MP-GC1009-Y033, CM Technology Company Ltd, Shenzhen, CN). The used VR device, Oculus Rift® (Oculus VR, Inc., Irvine, CA, USA), contains a number of micro-electrical-mechanical (MEMS) sensors including a gyroscope, accelerometer, and magnetometer. The information from each of these sensors is combined through the sensor fusion process to determine the motion of the user's head in the real world and synchronize the user's view in real-time [18]. Yaw, pitch, and roll data are acquired by utilizing Oculus software development kit (SDK) for Window released 1.26.0 provided by OCULUS VR on Microsoft Windows'10 and the sampling frequency is set to 44.59 Hz [19]. In order to control the ECS by the face rotation, the orientation data of VR headset acquired through Visual C++ 2015 (Microsoft Visual Studio Community 2015, version 14.0.25420.01, Microsoft, Redmond, WA, USA) are sent to LabVIEW® and the ECS is controlled according to the control algorithm developed on LabVIEW®. The specific control algorithm is described below.

2.2. VR control design

In a previous VR-based study [20], a command signal with a constant velocity was provided at angles larger than

threshold parameters. This approach provides a discontinuous velocity profile at the boundary of the threshold, and the actuator shows transient motion following a step function. Thus, an improved control design is required.

In this study, the pitch, yaw, and roll motions of the head were mapped to up/down, right/left, and roll view transitions. The control signals were generated based on the motion angles as follows:

$$\dot{\theta}_1 = sig(\theta_Y) \times k_Y \times f\{|\theta_Y - sig(\theta_Y) \times TH_Y|\}, \quad (1)$$

$$\dot{\theta}_2 = sig(\theta_P) \times k_P \times f\{|\theta_P - sig(\theta_P) \times TH_P|\}, \quad (2)$$

$$\dot{\theta}_3 = sig(\theta_R) \times k_R \times f\{|\theta_R - sig(\theta_R) \times TH_R|\}. \quad (3)$$

The function $f(x)$ indicates Rectified Linear Unit (ReLU), which is zero when $x < 0$, θ_Y, θ_P, and θ_R denote the yaw, pitch, and roll angles of the VR headset, respectively; TH_Y, TH_P, and TH_R denote the thresholds for the yaw, pitch, and roll motions, respectively; and θ_1 , θ_2, and θ_3 denote the angles of the ECS actuators for yaw, pitch, and roll motion of the endoscope, respectively. According to equations (1)–(3), the velocity of each actuator can be represented as shown in Fig. 2.

The speed of each motor is not activated within or outside the threshold, and the speed is designed to increase linearly as the angles of the head moves away from the boundary. Therefore, unintentional and minute movements of the user are ignored and the speed of motion can be adjusted according to the degree of head rotation of the user. The scaling coefficients k_Y, k_P, and k_R are empirically determined by considering usability and safety. In Fig. 2(c), the y-axis is the frontal direction of the user and the angle from the y-axis indicates the roll angle. The distance from the origin to the blue line corresponds to $\dot{\theta}_3$. The velocity $\dot{\theta}_3$ is activated when the head is rotated more than the threshold TH_R. When θ_R is too large, the situation is judged to be abnormal, and the operation is stopped since the angle is out of the normal rotation range of the human neck.

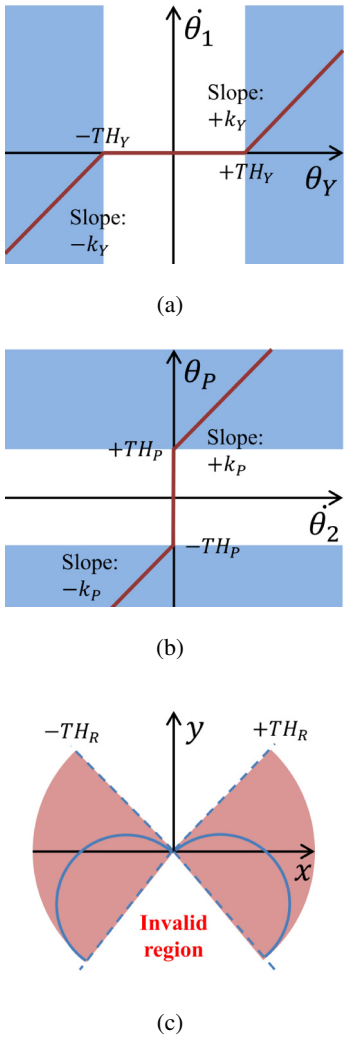

Fig. 2. Peg transfer task setup.

2.3. Validation of VR-based control

2.3.1 Peg transfer task

A peg transfer task suggested by the Fundamentals of Laparoscopic Surgery (FLS) is a conventional method of evaluating the hands-on skills of a surgeon. The standard peg transfer kit consists of a small pegboard with six rubber ring objects, as represented in Fig. 3. According to the rule suggested in the FLS [21], all six colored objects should be aligned on the six pegs on the same side of the boards as the non-dominant hand of the user. Firstly, the user grasps each object with his or her non-dominant hand and transfers the object mid-air to his or her dominant hand. Then, the object is placed on the peg on the opposite side of the pegboard. In the conventional version of the peg transfer task, the camera is adjusted to ensure that the field of view is centered on the pegboard and that the entire pegboard is visible. Thus, manipulation of the camera robot is not required. To test the VR-based control of the ECS, the conventional task was modified. The region of view is focused to show approximately 30% of whole pegboard, making control of the ECS necessary. For sim-

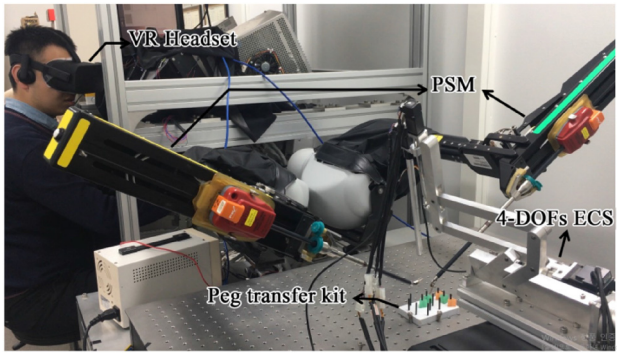

Fig. 3. Peg transfer task setup.

plicity, the task was modified so that motion that transfers the object to the opposite side of the pegboard occurs only in one direction. Four novice volunteers who had no experience in operating the dVRK and proposed VR-based ECS participated to identify the intuitiveness of the system, and the task was performed through four successive days. On each day, two trials of the task were performed. The time required for each trial was measured, and a learning curve was acquired.

2.3.2 Line tracking test

A line tracking test was also performed to validate the usability of the VR-based control. Intuitive and comfortable manipulation should provide consistent control efficiency regardless of the direction and curvature of the trajectory. Three trajectory shapes were used: a triangle, circle, and square with the same perimeter. The length of each trajectory was 40 cm. Circular markers were placed at equal intervals so that if the border was out of the range of view, the volunteer could start again based on the circle position (Fig. 4). The tracking started from the green circle, and the tracking direction (clockwise or counterclockwise) could be freely selected by the user. Four novice volunteers participated, and each shape was attempted three times (for a total of nine trials per volunteer). All volunteers were instructed that the line should not deviate from sight. The time required for each trial was measured.

2.4. Collision avoidance

The yaw and pitch motion control signals can cause collisions with other surgical end-effectors, so collisions should be avoided by additional intervention. When designing a collision avoidance strategy, it is important to generate a control signal that reflects both the intention of the user and collision avoidance simultaneously. Thus, the control command was generated by blending [22] the head motion and compensation signal as follows:

$$V_{compen} = \frac{k}{dist - (1+\beta) \times \frac{k_1+k_2}{2}} \times \frac{V_{\vartheta\varphi}}{\|V_{\vartheta\varphi}\|}, \tag{4}$$

$$V_{cmd} = \alpha \times V_{OCC} + (1-\alpha) \times \left(\frac{V_{compen,1} + V_{compen,2}}{2} \right), \tag{5}$$

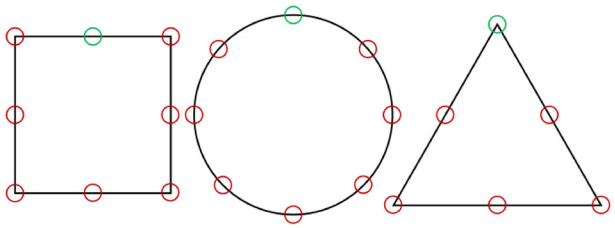

Fig. 4. Three simple shapes for the line tracking test.

$$V_{norm\_cmd} = V_{cmd} \times \frac{\|V_{OCC}\|}{\|V_{cmd}\|}. \tag{6}$$

Here, dist indicates the shortest distance between the baselines of two oriented bounding boxes (OBBs) of the endoscope and end-effector. $V_{\vartheta\varphi}$ is a vector designed to increase dist. The $V_{\vartheta\varphi}$ and OBB concepts and design approaches are described in detail in the following sections. The parameters k_1 and k_2 are the diagonal lengths (DLs) of the OBBs of the endoscope and end-effector, respectively. The parameter β ($= 0.1$ in the current study) is included as an additional collision buffer, and the parameter α indicates the blending proportion between the commands from Oculus (V_{occ}) and the two end-effectors ($V_{compen,1}$ and $V_{compen,2}$). The blended velocity vector (V_{cmd}) indicates the integrated command for the robotic endoscope. The final command signal is normalized to the size of V_{occ} because the second term of (5) ranges from zero to infinity. The compensation based on (4)-(6) is applied only when dist is less than the threshold (TH).

Theoretically, as the distance between the OBBs of the endoscope and end-effector approaches the buffer range, V_{compen} diverges to positive infinity, so that V_{occ}, which reflects the human intention in (5), is suppressed and the size of the second term (repulsive compensation) dominates. Nevertheless, there are likely to be three possible reasons for collisions in practical situations. First, if the frequency of the command signal is insufficient, collision avoidance does not work as a continuous model. Second, due to the control limitations, the hardware may not be able to follow the trajectory required by the proposed algorithm perfectly. Finally, V_{compen} of end-effectors 1 and 2 can cancel one another, in which case the second term of (5) does not work for collision avoidance.

2.5. OBB

In this section, the details of OBB are introduced. The curved and complicated shapes of surgical end-effectors are difficult to model mathematically for computation. Instead, by defining an OBB containing the surgical tool, the possibility of collision between the actual surgical end-effectors can be estimated by computing the likelihood of collision between the boxes [23]. The possible collision area (PCA) of the surgical end-effectors can be found by computing the intersection area between the OBBs. The OBB can be defined with three parameters: the starting point (SP), final point (FP), and DL, as represented in Fig. 5.

In the case of the endoscope and end-effectors, SP is defined as the center of the trocar and FP is defined as the end point of the end-effectors. DL is designed to be the minimum size that can include the surgical end-effectors. The dist can be computed based on the logic shown below [23]:

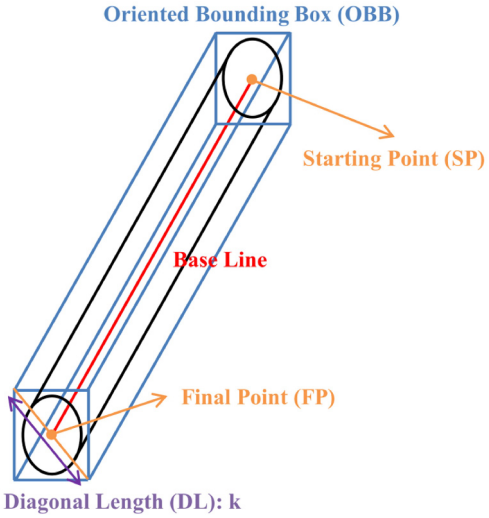

Fig. 5. OBB surrounding a cylindrical shape and three parameters, SP, FP, and DL, for defining OBB.

$$\text{dist}(L_i, L_j) = \begin{cases} \text{Case 1: } \|P_1 - P_2\| \\ \quad (\text{if } P_1 \in L_i \text{ and } P_2 \in L_j), \\ \text{Case 2: } \min\{\|A - P_2\|, \|B - P_2\|\} \\ \quad (\text{if } P_1 \in L_i^C \text{ and } P_2 \in L_j), \\ \text{Case 3: } \min\{\|C - P_1\|, \|D - P_1\|\} \\ \quad (\text{if } P_1 \in L_i \text{ and } P_2 \in L_j^C), \\ \text{Case 4: } \min\{\|A - C\|, \|A - D\|, \|B - C\|, \\ \quad \|B - D\|\} \\ \quad (\text{if } P_1 \in L_i^C \text{ and } P_2 \in L_j^C), \end{cases} \tag{7}$$

$$\text{Collision Index (CI)} = \text{dist}(L_i, L_j) - \frac{k_i + k_j}{2}, \tag{8}$$

where $\| * \|$ indicates the Euclidean distance between two points. L_i and L_j indicate the base lines of OBBs i and j, respectively, where the end points of L_i are A and B and the end points of L_j are C and D. The intersection points between the common perpendicular line and lines L_i and L_j are points P_1 and P_2, respectively. k_i and k_j are the DLs of OBBs i and j, respectively.

It can be confirmed that two OBBs with $\text{dist}(L_i, L_j) > \frac{k_i+k_j}{2}$ do not overlap, and a PCA does not exist. $\text{dist}(L_i, L_j) > \frac{k_i+k_j}{2}$ guarantees collision prevention even though it is not the strictest condition of OBB separation, which was described in a previous report [23]. Thus, a negative CI indicates that a PCA can exist (necessary condition) and a high possibility of collision is expected. As shown in Fig. 6(a), a boundary can be defined with a cylinder circumscribing the OBB and hemispheres at both ends. The radii of the cylinder and hemisphere are $\frac{DL}{2} = \frac{k}{2}$. In the four cases described in (7), two defined boundaries

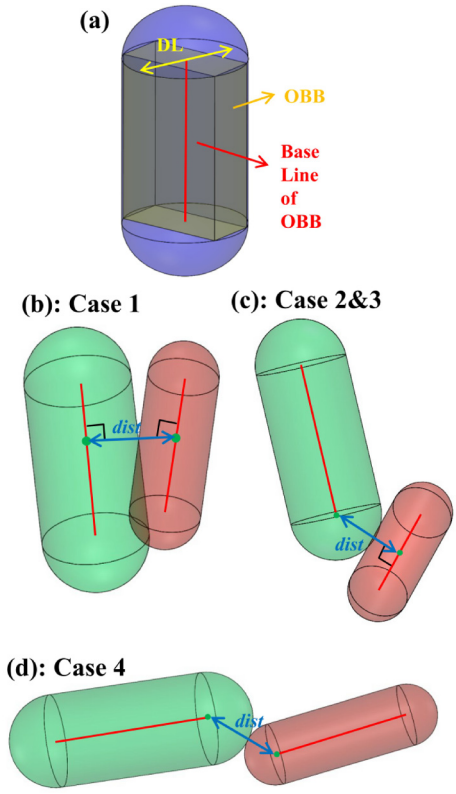

Fig. 6. (a) Cylinder circumscribing an OBB. (b) Case 1, (c) Case 2&3, and (d) Case 4 when *dist* (L_i, L_j) = (k_i + k_j)/2. Case 1 refers to the contact of two cylinders on the side, Case 2&3 refers to cases in which the hemisphere and cylinder are tangent, and Case 4 indicates that two hemispheres are in contact.

of OBBs are touching at a point when $\text{dist}(L_i, L_j = \frac{k_i+k_j}{2}$, as shown in Figs. 6(b)-(d). Thus, the OBBs inside the boundary cannot intersect when $\text{dist}(L_i, L_j) \geq \frac{k_i+k_j}{2}$.

2.6. Compensation vector calculation

Using the OBB concept, V_{compen} can be derived by projecting the increases in dist between the two base lines into θ and φ space (Figs. 7(a) and (b)). According to the logic of (7), a point P_{endo} on the endoscope base line and another point $P_{End-eff}$ on the surgical end-effector base line where the distance between the two points is minimized can be obtained. Using the two points, V_{compen} can be computed as shown below:

$$\begin{bmatrix} \hat{r} \\ \hat{\theta} \\ \hat{\varphi} \end{bmatrix} = \begin{bmatrix} \sin\theta\cos\varphi & \sin\theta\sin\varphi & \cos\theta \\ \cos\theta\cos\varphi & \cos\theta\sin\varphi & -\sin\theta \\ -\sin\varphi & \cos\varphi & 0 \end{bmatrix} \begin{bmatrix} \hat{y} \\ \hat{z} \\ \hat{x} \end{bmatrix}$$

$$= A \begin{bmatrix} \hat{y} \\ \hat{z} \\ \hat{x} \end{bmatrix}, \tag{9}$$

$$P_{End-eff} - P_{Endo} = a\hat{x} + b\hat{y} + c\hat{z}, \tag{10}$$

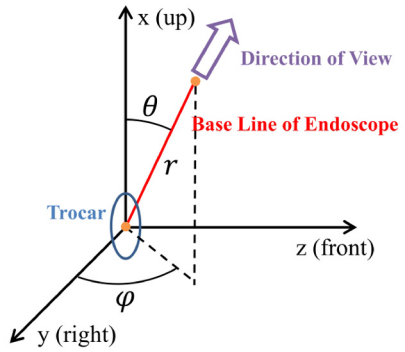

(a)

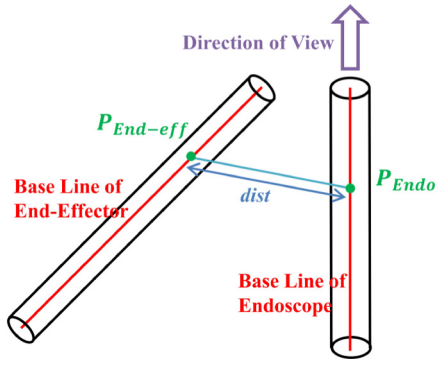

(b)

Fig. 7. (a) Definition of coordinates and angles θ and φ, (b) dist between the base lines of the end-effector and endoscope.

$$a\hat{x}+b\hat{y}+c\hat{z}=\begin{bmatrix} b & c & a \end{bmatrix}\begin{bmatrix}\hat{y}\\ \hat{z}\\ \hat{x}\end{bmatrix}=B\begin{bmatrix}\hat{y}\\ \hat{z}\\ \hat{x}\end{bmatrix}$$

$$=BA^{-1}\begin{bmatrix}\hat{r}\\ \hat{\theta}\\ \hat{\varphi}\end{bmatrix}=\begin{bmatrix} V_r & V_\theta & V_\varphi \end{bmatrix}\begin{bmatrix}\hat{r}\\ \hat{\theta}\\ \hat{\varphi}\end{bmatrix}, \quad (11)$$

$$V_{\theta\varphi}=V_\theta\hat{\theta}+V_\varphi\hat{\varphi}. \quad (12)$$

By using $V_{\theta\varphi}$ derived from (12), V_{compen} can be calculated using (4). In terms of control, collision should be avoided by controlling angles θ and φ. Thus, V_r in (11) is ignored in (12).

The collision avoidance strategy described in the above sections is applied only when the endoscope is within a certain rang from the surgical end-effector. Thus, the compensated control command in (6) is applied only when dist< TH. Otherwise, V_{occ} is directly input as a command signal.

2.7. Validation of collision avoidance

To verify the collision avoidance strategy, a computer-aided simulation using MATLAB® (R2018a, Mathworks Inc., Natick, MA, USA) was conducted instead of applying the strategy to actual hardware since the donated dVRK does not provide real-time end-effector position data. Computer-aided simulations are advantageous because they provide more objective information. In the simulation, pseudo-signals consisting of control variables θ and φ were provided. The settings of the required parameters are listed in Table 1, and the physical conditions used in the simulation are summarized in Table 2.

Table 1. Parameter settings of collision avoidance simulation.

Parameter	Unit	Value	Reference equation
k	-	0.0005	(4)
β	-	0.1	(4)
α	-	0.2-1.0 (interval of 0.2)	(5)
TH	m	0.03	-

*Parameters: k (diagonal length), β (collision buffer), α (blending proportion), and TH (threshold)

Table 2. Physical conditions of collision avoidance simulation.

Condition	Unit	Value	Reference equation
d_1 (Diameter of sugical end-effector)	m	0.0083	-
$k_1=\sqrt{2}d_1$ (DL of surgical end-effector)	m	0.01174	(4)
d_2 (Diameter of endoscope)	m	0.0140	-
$k_2=\sqrt{2}d_2$ (DL of endoscope)	m	0.01980	(4)
SP of endoscope	m	[0 0 0]	-

*Abbreviation: DL (diagonal length), SP (starting point)

To confirm the collision avoidace performance, the simulated robotic endoscope was commanded to move according to preprogrammed pseudo-signals and proposed control strategy, and the test was repeated with different values of α ranging from 0.2 to 1.0 in intervals of 0.2. At $\alpha = 1.0$, only the command signal from Oculus was reflected, and collision avoidance was not a concern. As α decreases, the involvement of the collision avoidance algorithm increases.

3. RESULTS

3.1. Evaluation of VR-based control

In the peg transfer task, the time for each trial decreased throughout the trials for each user, as shown in Fig. 8 and Table 3. The mean time decreased from 402.3 s (first trial) to 172.1 s (eighth trial). From the first to fourth trial,

the time decreased rapidly according to the learning curve (Fig. 8). The difference between users was not large except for one user (Volunteer 4). When the data of Volunteer 4 were excluded, the standard deviation (SD) of the other three users was 12.74 s at the final trial, which is just 7.4% of the mean execution time.

The execution times of the line tracking test are listed in Table 4. The average execution time among the users was 50.3 s in the first trial and decreased to 46.2 s and 45.4 s in the second and third trials, respectively. The users were able to track the line with a speed of 0.88 cm/s in the third trial. Furthermore, the SD of the execution times for different shapes was 3.63 s on average, which is only 8.0% of the total time consumed. In the third trial, triangular tracking required the least time (=42.75 s), while circular and square tracking required 46.25 s and 47.25 s, respectively.

3.2. Evaluation of collision avoidance

For the computer-aided simulation, the additionally required conditions are summarized in Tables 5 and 6. The simulations were conducted twice (simulations 1 and 2) with two different sets of conditions.

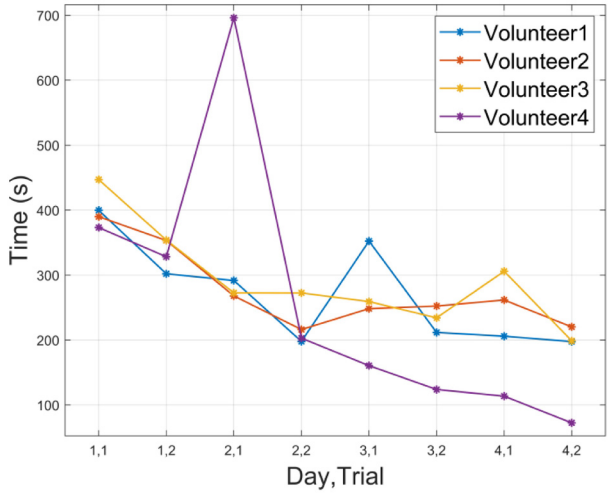

Fig. 8. Execution times of peg transfer task.

Table 3. Execution times of peg transfer task.

(Day, trial)	Volunteer no.				Mean	SD
	1	2	3	4		
(1,1)	389.85	399.56	446.87	373.08	402.34	30.51
(1,2)	353.11	301.98	353.83	328.11	334.26	29.73
(2,1)	267.80	291.48	272.51	696.03	381.96	12.54
(2,2)	216.06	197.73	272.33	202.74	222.22	38.87
(3,1)	248.20	352.31	259.07	160.44	255.01	57.23
(3,2)	252.19	211.58	234.04	123.74	205.39	20.34
(4,1)	261.52	205.76	305.78	113.43	221.62	50.12
(4,2)	220.07	197.42	198.63	72.27	172.10	12.74

*Unit: Seconds, Abbreviation: SD (standard deviation)

Table 4. Execution times of line tracking test.

	Volunteer 1			Volunteer 2		
Trial	1	2	3	1	2	3
Circle	54	47	52	48	45	48
Triangle	58	50	44	48	49	42
Square	48	47	47	43	45	48
Mean	53	48	48	46	46	46
SD	5	2	4	3	2	3
	Volunteer 3			Volunteer 4		
Trial	1	2	3	1	2	3
Circle	48	39	33	54	53	52
Triangle	50	41	36	52	51	49
Square	42	35	41	59	52	53
Mean	47	48	37	55	52	51
SD	4	3	4	4	1	2

*Unit: Seconds, Numbers are shown after round-off, Abbreviation: SD (standard deviation)

Table 5. Additional conditions for simulation 1.

Condition	Unit	Value
SP of surgical end-effector 1	m	[-0.05 0.05 0]
FP of surgical end-effector 1	m	[0 0 0.1]
SP of surgical end-effector 2	m	[0.05 0.05 0]
FP of surgical end-effector 2	m	[0 0.06 0.1]
Initial value of θ	rad	$\frac{\pi}{2}$
Increment per epoch of θ	rad	0
Initial value of φ	rad	$\frac{\pi}{8}$
Increment epotch of φ	rad	$\frac{\pi}{200}$
Total epoch	-	100

*Abbreviation: SP (starting point), FP (final point)

Table 6. Additional conditions for simulation 2.

Condition	Unit	Value
SP of surgical end-effector 1	m	[-0.05 0.05 0]
FP of surgical end-effector 1	m	[0 0 0.1]
SP of surgical end-effector 2	m	[0.05 0.05 0]
FP of surgical end-effector 2	m	[0.02 0.05 0.1]
Initial value of θ	rad	$\frac{\pi}{2}$
Increment per epoch of θ	rad	$-\frac{\pi}{400}$
Initial value of φ	rad	$\frac{\pi}{4}$
Increment epotch of φ	rad	0
Total epoch	-	100

*Abbreviation: SP (starting point), FP (final point)

The results of simulation 1 are presented in Fig. 9. According to the graph, compensation for collision was applied when dist$<$ TH (brown line), and dist less than the red line indicates points at which collision is immediately possible. As α increases, the minimum dist during the

simulation tends to increase. In particular, dist is less than collision level (red line) when compensation was not applied ($\alpha = 1$), and collision did not occur when $\alpha < 1.0$ since the compensation signal for ollision avoidance was blended. When $\alpha \leq 0.4$, thecompensation for collision avoidance was applied too much, and dist does not decrease below the brown line.

The simulation was repeated with finer modification of α. The additional simulation was repeated by increasing α from 0.4 to 0.6 in increments of 0.05, and the results are presented in Fig. 10. The graph shows that dist oscillates at a specific equilibrum point when $\alpha < 0.6$. The equilibrium dist occurs at a higher point as α decreases since larger repulsive compensation was blended.

Figs. 11(a)-(c) present the endoscope trajectories in the cases of $\alpha = 0.40$, 0.60, and 1.0. It can be confirmed that in case of $\alpha = 0.4$, the endoscope did not move as commanded by the pseudo-signal because the repulsive compensation from the two surgical end-effectors was sufficiently strong to resist the pseudo-signal. The repulsive compensation from the two end-effectors and the control signal were equilibrated and a local minimum was formed. As shown in Fig. 10, the lower the blended proportion of collision avoidance, the weaker the repulsive force, and the closer the equilibrium point could be to the end-effectors.

The same process was repeated for the conditions in simulation 2, and the results are presented in Fig. 12. A collision can occur when $\alpha = 1.0$ but is avoided when $\alpha < 1.0$.

The additional simulation was repeated by increasing α from 0.6 to 0.8 in increments of 0.05, and the results are shown in Fig. 13. As α decreases, it becomes more difficult to approach the end-effector closely since the repulsive effect is greater. When $\alpha \leq 0.60$, dist oscillates near TH (brown line) because the repulsive effect is sufficiently strong.

Figs. 14(a)-(c) depict the endoscope trajectories corresponding to $\alpha = 0.40$, 0.80, and 1.0. As shown in this figure, the endocope collides head-on when $\alpha = 1.0$, since no compensation is applied. When $\alpha = 0.80$, collision is avoided, and dist simultaneously approaches 1.56 cm (0.91 cm from the red line). However, when $\alpha = 0.40$, the endoscope cannot approach the endoscope sufficiently closely because of the relatively strong repulsive compensation.

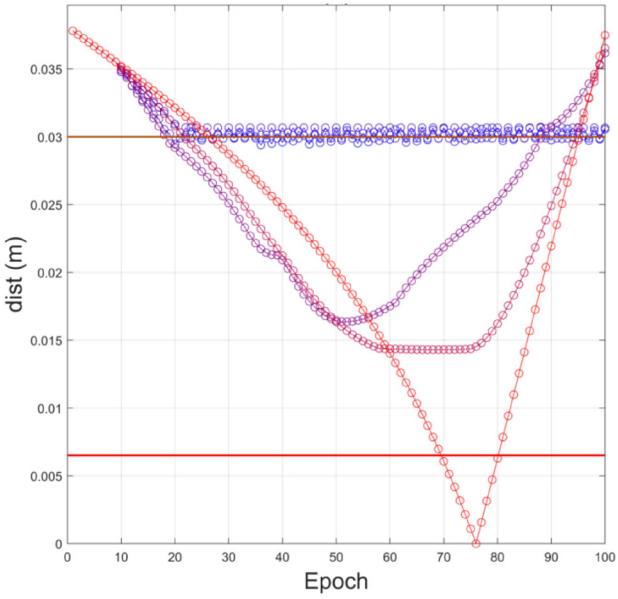

(a)

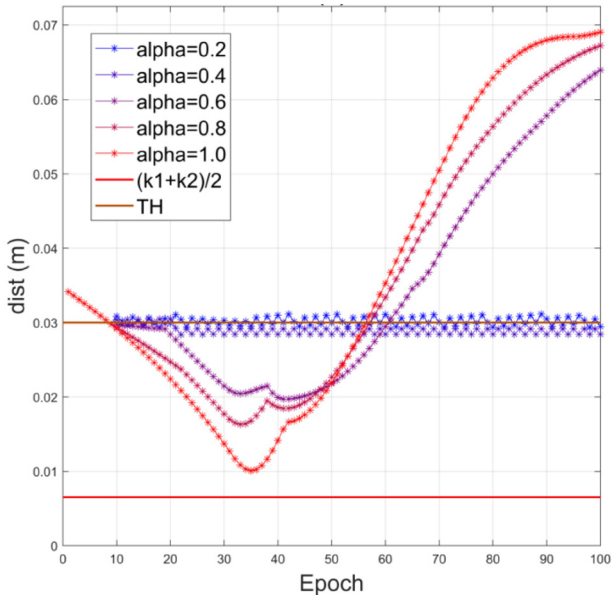

(b)

Fig. 9. dist when α was changed from 0.2 to 1.0 (simulation 1). (a) dist between endoscope and end-effector 1. (b) dist between endoscope and end-effector 2.

4. DISCUSSION

In this study, an ECS was controlled using a VR headset. This approach is highly advantageous compared to the previous techniques because a large and heavy stereo viewer can be eliminated and intuitive control is possible. The roll, pitch, and yaw motions of the head were mapped to the corresponding ECS motions, and the performance was tested by applying the proposed method in a peg transfer task and line tracking test. In the peg transfer task, the users reduced the execution time quickly as the trial was repeated. In only eight trials, the execution time decreased by 57.2% on average from the first trial. In particular, the execution time decreased by 44.8% from

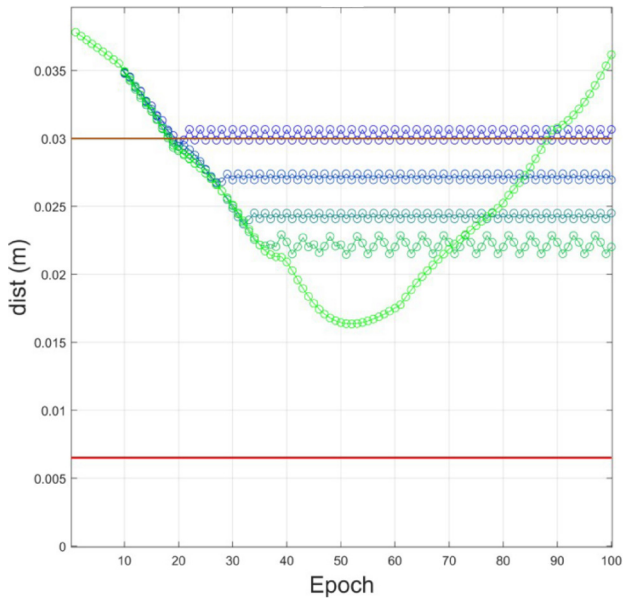

(a)

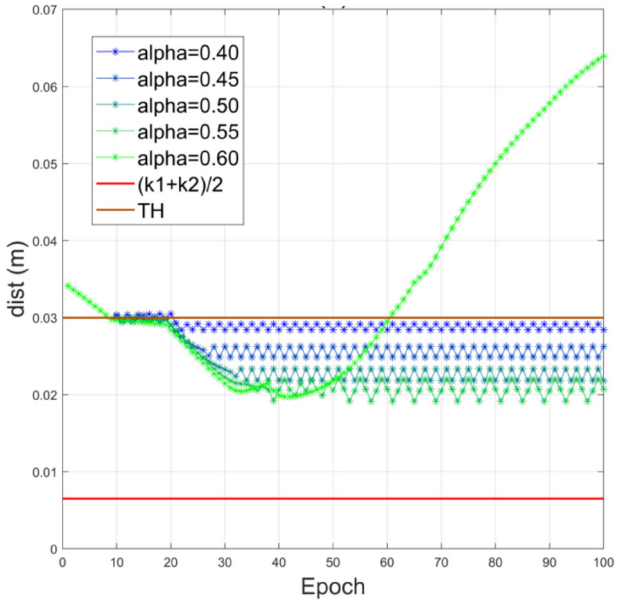

(b)

Fig. 10. dist when α changes from 0.40 to 0.60 (simulation 1). (a) dist between endoscope and end-effector 1. (b) dist between endoscope and end-effector 2.

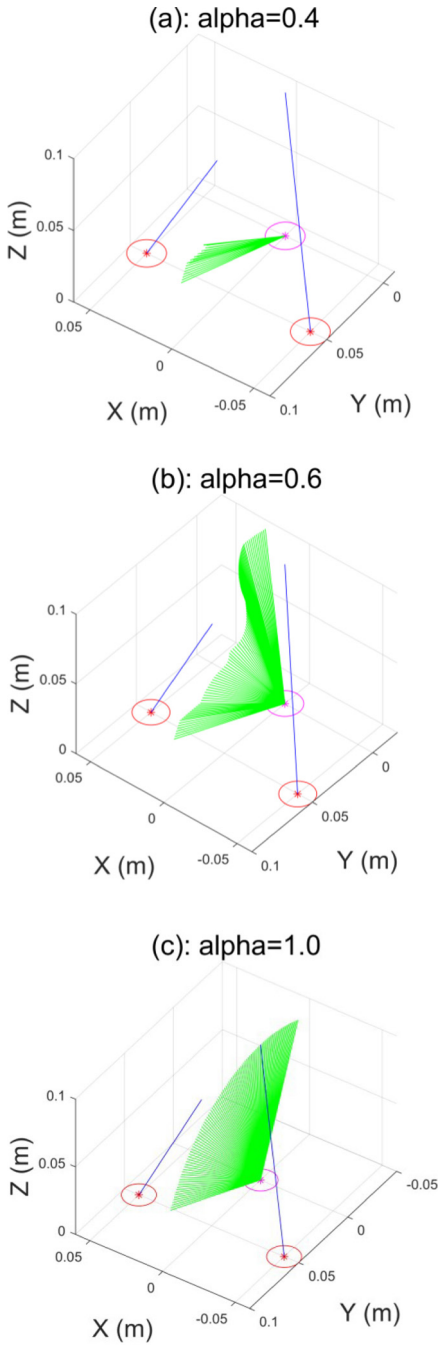

Fig. 11. Endoscope trajectory when α is (a) 0.4, (b) 0.6, and (c) 1.0 (simulation 1).

the first to fourth trial. These findings indicate that the proposed system does not require a long training period for adjustment, and most of training effect is saturated in only four trials. Furthermore, the inter-user variability was small (SD= 7.4%), when one subject (Volunteer 4) was excluded. For the three users, it is confirmed that not only patterns of decreasing execution time but also absolute execution time are similar (Fig. 8 and Table 3). The small inter-user variability in absolute value indicates that the proposed system provides consistent performance regardless of the user. In the case of Volunteer 4, the learning curve saturated to a significantly better point than it did for the other users. It seems that the user had a natural talent for manipulating the sophisticated instruments compared to the other novice volunteers.

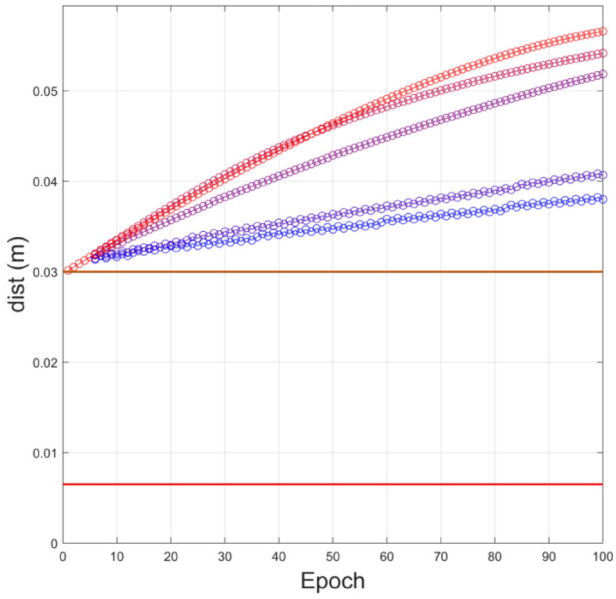

(a)

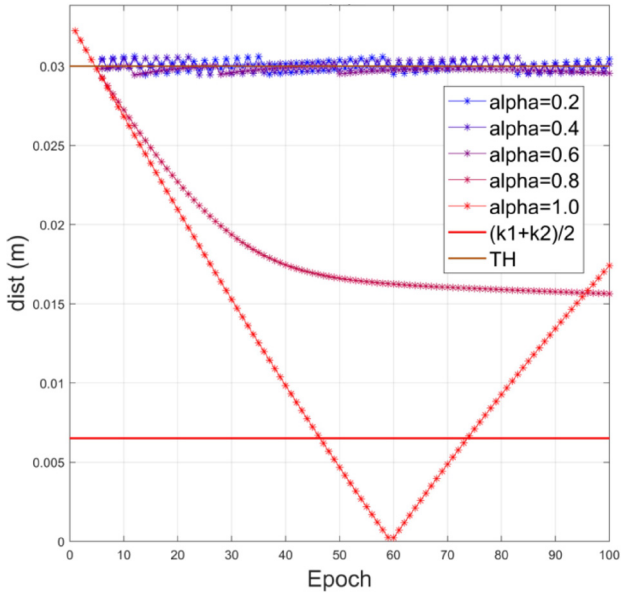

(b)

Fig. 12. dist when α changes from 0.2 to 1.0 (simulation 2). (a) dist between endoscope and end-effector 1. (b) dist between endoscope and end-effector 2.

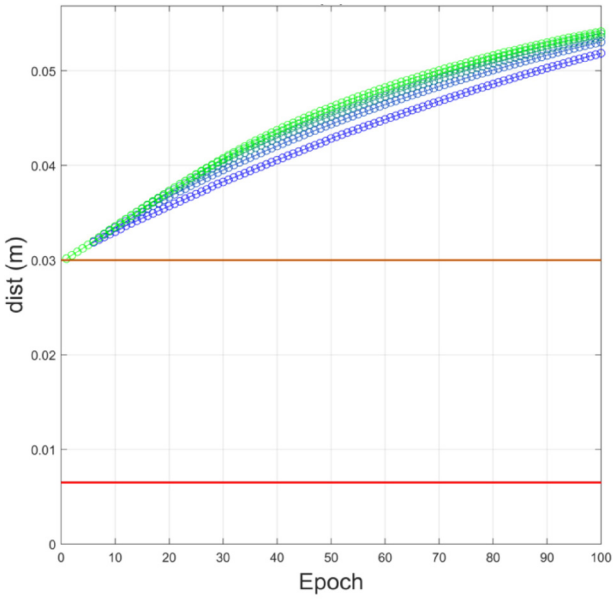

(a)

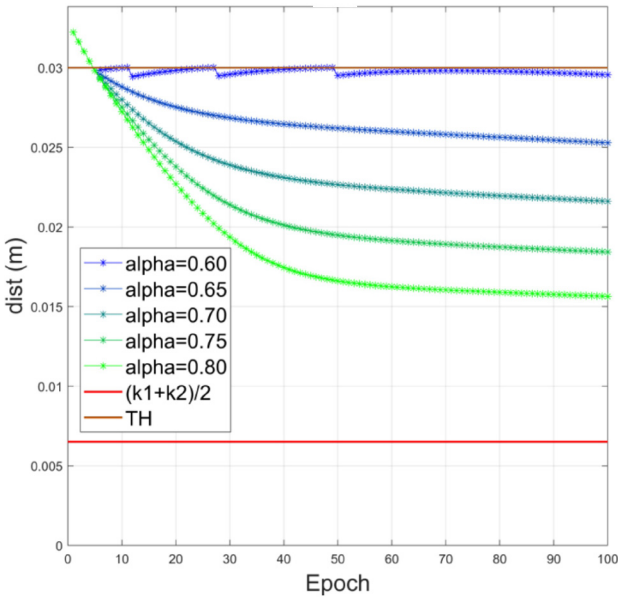

(b)

Fig. 13. dist when α changes from 0.60 to 0.80 (simulation 2). (a) dist between endoscope and end-effector 1. (b) dist between endoscope and end-effector 2.

A line tracking test was also performed to validate the developed system. All of the users commented that the system was highly intuitive and convenient for line tracking. The learning phase was not obviously observed because the execution time decreased slightly as the trials were repeated. Compared to the initial time, the time for the third trial was reduced by only 9.8%. We believe that the decrease in execution time was slight since the users were sufficiently trained during previously performed peg transfer task. Additionally, the line tracking test does not include the manipulation of dVRK and only requires the VR-based control of ECS. For this reason, it can be considered that the line tracking test is easier than the peg

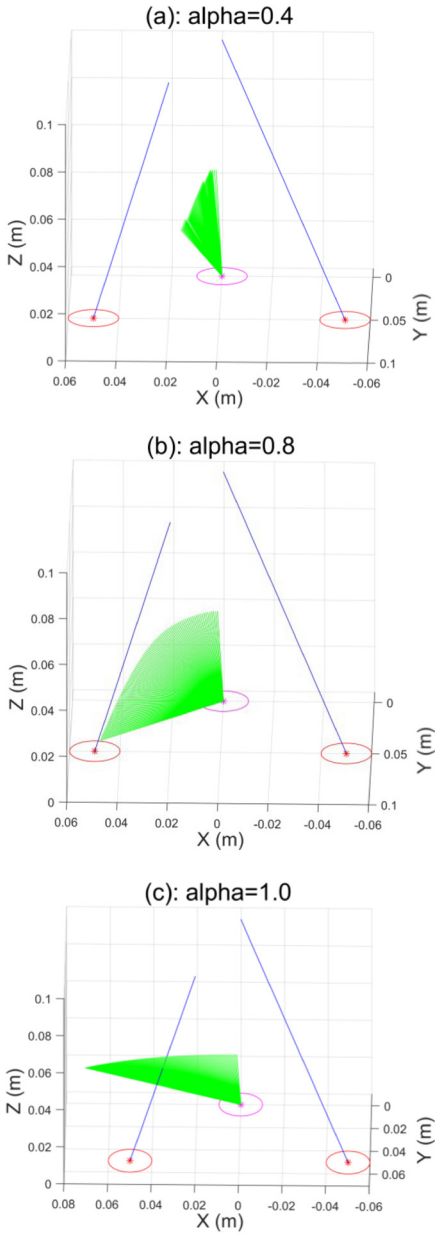

Fig. 14. Endoscope trajectory when α is (a) 0.4, (b) 0.8, and (c) 1.0 (simulation 2).

transfer task. Users also commented that the control of ECS without dVRK was an easier task and additional training did not seem to be required for further improvement in reducing the execution time. The small SD among the different shapes in the third trial indicates that the control performance does not depend significantly on the direction or curvature of the trajectory. Among the three shapes, the shortest time was required for the triangular trajectory because fewer directional changes were needed than in the other cases.

The collision issue was addressed in depth in this study even though the developed algorithm was not employed for real-time control. The suggested collision avoidance strategy can prevent collisions between the ECS and surgical end-effectors. The large repulsive compensation generated by a small α guarantees a safe surgical environment. However, unconstrained ECS motion controlled by user manipulation can be interrupted because of an unwanted repulsive effect. Thus, collision prevention and unconstrained manipulation have a trade-off relationship. According to the simulation results, no collision occurred when $\alpha < 1$, because the repulsive compensation diverged to an extremely large value as dist converged to the collision level. However, in a practical system, the theoretical prediction is not always achieved due to the command signal frequency and time latency limitations. Consequently, α should be determined with an additional margin. The proper range for α can be considered to be 0.70-0.90 when an additional margin is considered. $\alpha < 0.65$ shows local minima when the net user control command and repulsive comensation are in equilibrium. As α increases, the user command becomes dominant and closer approach is allowed. At least two simulations did not show local minima or collisions within the suggested range of α. It is expected that more systematic and numerous simulations should be designed and conducted to search for a more validated range of α.

5. CONCLUSION

In this research, VR-based control of an ECS is suggested for an enhanced and efficient ergonomic robot-assisted surgery. Specifically, in the proposed system, a VR device built-in AHRS module could replace a stereo viewer in the dVRK and control 3D endoscope. The novice volunteers exhibited rapid learning in the peg transfer task and little inter-user variability with the developed system. Furthermore, the ECS was able to follow the lines of three different shapes and the differences among the execution times were slight. These findings indicate that the control of the suggested system hardly depends on the direction or curvature of the followed path. Finally, a collision avoidance strategy for VR-based ECS control was suggested and validated by performing a simulation. Based on the simulation results, a proper range of the required parameter for safe and less constrained control of the ECS was identified. Therefore, the proposed system could improve the intuitiveness and safety of surgery and contribute to size reduction of robotic surgical systems. Also, the ergonomic VR-based ECS proposed in this research could reduce surgeon's pains in both neck and back which potentially greatly reduce surgeon's workload during the surgery.

REFERENCES

[1] G. H. Ballantyne, "Robotic surgery, telerobotic surgery,

telepresence, and telementoring," *Surgical Endoscopy And Other Interventional Techniques*, vol. 16, no. 10, pp. 1389-1402, October 2002.

[2] A. T. Ng and P. C. Tam, "Current status of robot-assisted surgery," *Hong Kong Medical Journal*, vol. 20, no. 3, pp. 241-250, May 2014.

[3] T. E. Ahlering, D. Sharecky, D. Lee, and R. V. Clayman, "Successful transfer of open surgical skills to a laparoscopic environment using a robotic interface: initial experience with laparoscopic radical prostatectomy," *The Journal of Urology*, vol. 170, no. 5, pp. 1738-1741, November 2003.

[4] V. Ficarra, G. Novara, W. Artibani, A. Cestari, A. Galfano, M. Graefen, G. Guazzoni, B. Guillonneau, M. Menon, F. Montorsi, V. Patel, J. Rassweiler, and H. Van Poppel, "Retropubic, laparoscopic, and robot-assisted radical prostatectomy: A system review and cumulative analysis of comparative studies," *European Urology*, vol. 55, no. 5, pp. 1037-1063, May 2009.

[5] J. P. Ruurda, T. J. van Vroonhoven, and I. A. Broeders, "Robot-assisted surgical systems: a new era in laparoscopic surgery," *Annals of the Royal College of Surgeons of England*, vol. 84, no. 4, pp. 223-226, July 2002.

[6] J. Finkelstein, E. Eckersberger, H. Sadri, S. S. Taneja, H. Lepor, and B. Djavan, "Open versus laparoscopic versus robot-assisted laparoscopic prostatectomy: The European and US experience," *Reviews in Urology*, vol. 12, no. 1, pp. 35-43, 2010.

[7] O. A. J. van der Meijden and M. P. Schijven, "The value of haptic feedback in conventional and robot-assisted minimal invasive surgery and virtual reality training: a current review," *Surgical Endoscopy*, vol. 23, no. 6, pp. 1180-1190, June 2009.

[8] G. Turchetti, F. Pierotti, and A. Cuschieri, "Economic evaluation of da Vinci-assisted robotic surgery: a systematic review," *Surgical Endoscopy*, vol. 26, no. 3, pp. 598-606, March 2012.

[9] C. W. Kim, C. H. Kim, and S. H. Baik, "Outcomes of robotic-assisted colorectal surgery compared with laparoscopic and open surgery: a systematic review," *Journal of Gastrointestinal Surgery*, vol. 18, no. 4, pp. 816-830, April 2014.

[10] A. Ahmad, Z. F. Ahmad, J. D. Carleton, and A. Agarwala, "Robotic surgery: current perceptions and the clinical evidence," *Surgical Endoscopy*, vol. 31, no. 1, pp. 255-263, January 2017.

[11] J. B. Gomez, A. Ceballos, F. Prieto, and T. Redarce, "Mouth gesture and voice command based robot command interface," *Proc. of the Conf. IEEE International Conference on Robotics and Automation (ICRA)*, July 2009.

[12] N. Hong, M. Kim, C. Lee, and S. Kim, "Head-mounted interface for intuitive vision control and continuous surgical operation in a surgical robot system," *Medical & Biological Engineering & Computing*, vol. 57, no. 3, pp. 601-614, March 2019.

[13] M. Kim, C. Lee, W. Park, Y. S. Suh, H. K. Yang, H. J. Kim, and S. Kim, "A development of assistant surgical robot system based on surgical operation-by-wire and hands-on-throttle-and-stick," *Biomedical Engineering Online*, vol. 15, no. 58, May 2016.

[14] M. Kim, C. Lee, N. Hong, Y. J. Kim, and S. Kim, "Development of stereo endoscope system with its innovative master interface for continuous surgical operation," *Biomedical Engineering Online*, vol. 16, no. 81, pp. 1-16, June 2017.

[15] Y. Cao, S. Miura, Y. Kobayashi, K. Kawamura, S. Sugano, and M. G. Fujie, "Pupil variation applied to the eye tracking control of an endoscopic manipulator," *IEEE Robotics and Automation Letter*, vol. 1, no. 1, pp. 531-538, January 2016.

[16] T. Kawai, M. Fukunish, A. Nishikawa, Y. Nishizawa, and T. Nakamura, "Hands-free interface for surgical procedures based on foot movement patterns," *Proc. of the 36th Conf. Annual International Conference of the IEEE Engineering in Medicine and Biology Society*, pp. 345-348, November 2014.

[17] M. M. Lux, M. Marshall, E. Erturk, and J. V. Joseph, "Ergonomic evaluation and guidelines for use of the DaVinci robot system," *Journal of Endourology*, vol. 24, no. 3, March 2010.

[18] Oculus VR, "Initialization and Sensor Enumeration," https://developer.oculus.com/documentation/pcsdk/latest/concepts/dgsensor/, Accessed May 29, 2018.

[19] Y. Jo, Y. J. Kim, H.-M. Moon, and S. Kim, "Development of virtual reality-vision system in robot-assisted laparoscopic surgery," *Proc. of the 18th Conf. International Conference on Control, Automation and System*, pp. 1708-1712, 2018.

[20] K. Zinchenko, O. Komarov, and K. T. Song, "Virtual reality control of a robotic camera holder for minimally invasive surgery," *Proc. of the 11th Conf. Asian Control Conference*, pp. 970-975, February 2017.

[21] Fundamentals of Laparoscopic Surgery, "FLS manual skills written instructions and performance guideline," https://www.unmc.edu/surgery/residencies-fellowships/mis-fellowships/training/manual-skills-guidelines-for-cd.pdf, Accessed January 2019.

[22] Y. J. Kim, H. S. Nam, W. H. Lee, H. G. Seo, J.-H. Leigh, B.-M. Oh, M. S. Bang, S. Kim, "Vision-aided brain-machine interface training system for robotic arm control and clinical application on two patients with cervical spinal cord injury," *BioMedical Engineering Online*, vol. 18, no. 14, February 2019.

[23] Y. Qiu, Z. Yan, Y. Miao, and Z. Du, "Real-time collision avoidance algorithm for surgical robot based on OBB intersection test," *Proc. of the 19th Conf. International Conference on Intelligent Robotics and Applications*, pp. 195-205, August 2017.

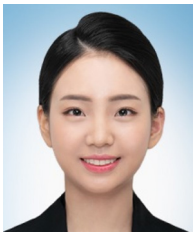

Yeeun Jo received her B.S. degree in Biomedical Engineering from Gachon University in 2017. She is currently pursuing an M.S. degree in the Interdisciplinary Program for Bioengineering from Seoul National University. Her research interests include robotic system.

Yoon Jae Kim received his B.S. degree in Mechanical & Aerospace Engineering from Seoul Nation University (SNU) in 2014 and his Ph.D. degree in the Interdisciplinary Program for Bioengineering from Seoul National University in 2018. He is a researcher at Institute of Medical and Biological Engineering, SNU. His research interests include development of robotic hardware and algorithms.

Minwoo Cho received his B.S. degree in Electronics Engineering from Kyungbook University in 2012 and an M.S. degree in the Interdisciplinary Program for Bioengineering from Seoul National University in 2014. He is currently pursuing a Ph.D. degree in the Interdisciplinary Program for Bioengineering from Seoul National University. His research interests include robotic system and Image processing.

Chiwon Lee received his B.S. degree in Mechanical & Aerospace Engineering and a Ph.D. degree in the Interdisciplinary Program for Bioengineering from Seoul National University, in 2011 and 2015. He is a senior researcher at Korea Electrotechnology Research Institute. His research interests include medical robot, machine learning, and 3D printing technology for medical applications.

Myungjoon Kim received his B.S. degree in Electronics Engineering from Tsinghua University in 2012 and his Ph.D. degree in the Interdisciplinary Program for Bioengineering from Seoul National University in 2017. He is a senior researcher at Korea Electrotechnology Research Institute. His research interests include development of medical robot system.

Hye-Min Moon received her B.S. degree in Addiction Rehabilitation Social Welfare from Eulji University, in 2017. She is currently an M.S. student in Bioengineering, Seoul National University. Her research interests include medical robot systems.

Sungwan Kim received his B.S. degree in Electronics Engineering and M.S. degree in Control & Instrumentation Engineering from Seoul National University (SNU), in 1985 and 1987, and his Ph.D. degree in Electrical Engineering from University of California at Los Angeles in 1993. He is a professor with the Department of Biomedical Engineering, SNU College of Medicine since 2010. Prior to joining to the SNU, he worked as a Senior Aerospace Engineer at National Aeronautics and Space Administration (NASA) Langley Research Center, USA. He is an Associate Fellow of the AIAA and a Senior Member of the IEEE.